A Modeling Study and Scaling Analysis of Orographic Effects on Boundary Layer Shallow Convection

WENSHOU TIAN AND DOUGLAS J. PARKER

Institute for Atmospheric Science, School of the Environment, University of Leeds, Leeds, United Kingdom

(Manuscript received 22 May 2002, in final form 6 March 2003)

ABSTRACT

Effects of orography on boundary layer shallow convection under various background winds are studied using a two-dimensional model together with scaling analysis. Under a motionless background state the flow response over a heated hill is a vortex pair, with one horizontal vortex over each slope. Additional lifting of the inversion by this vortex pair is estimated by w_t/N, with w_t being the intensity of the terrain-induced thermal circulation, and N the Brunt–Väisälä frequency, for which a simple expression is given based on heat engine framework. Modification of the CBL top by terrain-induced waves is quantified using linear gravity wave theory in a two-layer atmosphere configuration. These simple estimates of the CBL-top perturbation are found to be consistent with the model results when waves and convection dominate the flow pattern.

A convective core is found to occur over high hills when the winds are light, developing in the late afternoon when the CBL depth is high. A scaling is proposed to determine the existence of the convective core in terms of hill slope, background winds, boundary layer depth, and tropospheric stability.

The downstream modification of convection by terrain-related processes is also examined. Under light wind conditions, the reversed thermal circulation in the lee and corresponding downward motions may suppress thermal eddies in the vicinity of the lee of a hill.

1. Introduction

Observational and numerical studies have supplied convincing evidence that orography plays an important role in precipitation distribution over land (e.g., Smith and Lin 1982; Smolarkiewicz et al. 1988; Rowell and Milford 1993). It has been observed that convective cells form repeatedly in a fixed location relative to orography with most of them being generated by terrain-related processes (e.g., Akaeda et al. 1995; Tucker and Crook 1999). Among various orographic processes, forced ascent windward of orography, a leeside convergence line, terrain-induced gravity waves, and diurnal flow regimes are though to have potential impacts on the development of convective systems (e.g., Tripoli and Cotton 1989; Crook et al. 1990; Chu and Lin 2000). All of these mechanisms originate in the interaction between the terrain and the planetary boundary layer (PBL).

Influences of orography on convection are largely related to the scales of a hill and of the convection itself, as well as the background flow conditions. The richness of the flow regimes (e.g., Lin and Wang 1996) over orography, and complexity of the interaction between various physical processes, make it quite difficult to synthesize orographic effects on convection in a single frame. While previous studies have led to much progress in our understanding of orographic processes involved in mesoscale convective systems over relatively large orography, the orographic effects on boundary layer shallow convection over low hills of moderate slope have been less closely examined. Some authors (e.g., Walko et al. 1992; Gopalakrishnan et al. 2000) have studied the convective boundary layer (CBL) over small hills using large eddy simulations (LESs). Those LESs over small periodic model domains have revealed that orographic effects on the CBL depend on the scales of hill. It is the purpose of this study to understand and quantify the fundamental processes of orographic influence on the CBL, and the convective properties over mesoscale hills where LES is, in general, not feasible due to computational demands.

It is reckoned that, in the absence of thermal circulations and strong wind shear, flow over an isolated hill is controlled by a Froude number $\mathrm{Fr} = U/Nh$, where U is background wind, N is Brunt–Väisälä frequency, and h is the hill height). However, when the CBL is developed over a hill, thermal circulations may become important and it is necessary to clarify what kind of parameters are responsible for flow patterns over a hill in the presence of thermal convection.

Although much attention has been paid in previous

Corresponding author address: Dr. Douglas J. Parker, School of the Environment, University of Leeds, Leeds LS2 9JT, United Kingdom.
E-mail: doug@env.leeds.ac.uk

TABLE 1. Model configuration for different runs (where u_g is geostrophic wind; h and l are hill height and total width, respectively).

Configuration type	A0	A1	A2	B0	B1	B2	C0	C1	C2	C3
h (m)	0.0	200.0	500.0	0.0	200.0	500.0	0.0	200.0	500.0	500.0
l (km)	0.0	10.0	10.0	0.0	10.0	10.0	0.0	10.0	10.0	20.0
u_g (m s^{-1})	0.0	0.0	0.0	2.0	2.0	2.0	10.0	10.0	10.0	10.0

studies to flow responses over or in the vicinity of a single hill (e.g., McNider and Pielke 1981; Chen et al. 1996; and many others), systematic modification of convection downstream of a hill by terrain-related processes is not well addressed. The downstream modification of convection by terrain-induced gravity waves is, in particular, a subject of much debate and worth further investigation (e.g., Tripoli and Cotton 1989; Chu and Lin 2000).

The aim of this paper is to quantify the modification of the PBL over low hills in relation to convective initiation. In particular we investigate the lifting of the mixed-layer top by thermal and dynamic mechanisms, and the systematic downstream modification of the convective stability, as they are controlled by external flow parameters. The strategy employed here is to perform idealized model simulations together with theoretical analysis to determine how orography influences the development of the CBL. Instead of using constant thermal forcing at the model surface to find steady-state convective features over a periodic domain, the idealized simulations of a full life cycle of convection over an isolated hill under a diurnal thermal cycle are performed in this study. We will discuss the problem in three broad categories: motionless background state, light winds with weak or no waves, and high winds with significant waves.

2. Numerical experiments

We have used the Met Office boundary layer model called Boundary Layer Above Stationary, Inhomogeneous Uneven Surface (BLASIUS). Changes have been made to the model to include a radiation divergence term in the thermodynamic equation. A surface model is also incorporated to diagnose diurnal variation of the surface temperature T_g and humidity q_g. Note that, although water vapor is included in the model, condensation and latent heat release are not considered at present. More details of the model configuration are given in Tian and Parker (2002).

The model has been run in a two-dimensional configuration with a first-order turbulence closure scheme. The model configuration for 10 basic runs is listed in Table 1. All runs begin at 0600 UTC, when the model is initialized with the results of a one-dimensional simulation, and all last for 24 h. To depict more clearly the effects of the terrain, the large-scale geostrophic winds are unchanged throughout an integration. Coriolis parameter $f = 10^{-4}$ s^{-1} and the basic-state stability $N = 0.012$ s^{-1} are fixed for all runs.

The lateral boundary conditions for flat domain runs are periodic. For hilly terrain runs, the velocity at the inflow boundary is provided by the results from the corresponding flat terrain simulation while the temperature is treated using the zero gradient condition. The radiation boundary condition together with a tendency modification scheme of Davies (1983) was used at the outflow boundary in hilly terrain simulations. Adoption of such open boundary conditions makes it possible to detect any downstream modification of convection by isolated orography. A 10-km-deep domain is chosen and an artificial absorbing layer is added to the top of the model to reduce wave reflection. The domain length is 40 km in simulations A0, B0, and C0, and 60 km for all hilly terrain runs. In the course of analysis, the results over the inner 40-km region, on which two lateral boundaries are thought to have small effect, will be primarily considered. The results from a test run with an 80-km horizontal domain indicate that a 60-km horizontal domain is enough to avoid significant distortion of physical properties by the lateral boundaries. The horizontal resolution is 1 km, and the vertical mesh is stretched with 50 points: effects of resolution on similar simulations have been discussed by Tian and Parker (2002), and the bulk features of the boundary layer evolution have been found to be robust. Tian et al. (2003) describe validation of the model with field observations and it seems that the bulk properties of coherent boundary layer convective structures are well resolved.

A single hill is located with its summit 20 km from the upstream boundary of the model domain in hilly terrain runs, and its form satisfies

$$Z_s(x) = h \cos^2\left(\frac{\pi x}{l}\right), \qquad -\frac{l}{2} < x < \frac{l}{2}. \tag{1}$$

For the purpose of analysis, the governing equations describing an inviscid Boussinesq fluid are given as follows:

$$\frac{d\mathbf{u}}{dt} = -\nabla\phi - f\mathbf{k} \times \mathbf{u} - \mathbf{k}B, \tag{2}$$

$$\frac{d\theta}{dt} = Q\frac{\theta_0}{g}, \tag{3}$$

$$\nabla \cdot \mathbf{u} = 0, \tag{4}$$

where $\mathbf{u}$ is the wind vector, θ is the potential temper-

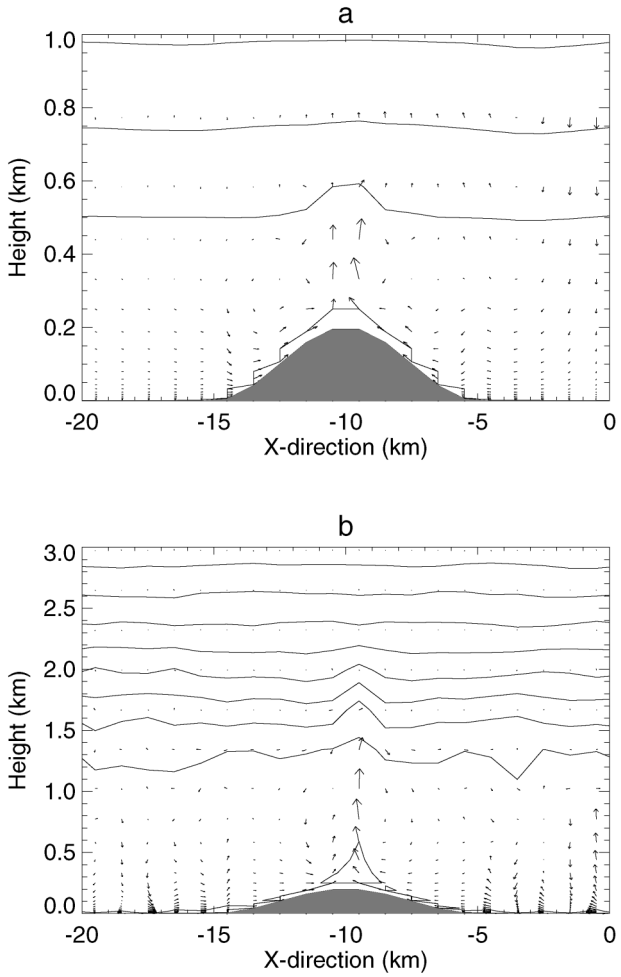

FIG. 1. The instantaneous wind vectors and the potential temperature fields at (a) 0900 and (b) 1300 UTC gathered from simulation A1. The contour interval for the potential temperature is 1.0 K. For clarity, different ranges of vertical coordinate are used for two plots.

ature, B denotes the buoyancy, θ_0 is a reference potential temperature, g is the gravitational constant, and Q is the thermal forcing. For the convenience of later use, Q is expressed as a buoyancy depletion rate in dimensions of acceleration over time.

3. Analysis of model results

a. Convergence over hilltop

Under a motionless background state, the flow responses to an obstacle are thermally dominated. Figure 1 depicts two model realizations of velocity and potential temperature fields from simulation A1. As the surface is heated gradually in the early morning (Fig. 1a), a convective upslope flow develops with a pair of vortices located over the two slopes of the ridge. The lifting of the air by the convergence over the summit of the hill is readily seen. The CBL continues to grow in both the vertical and the horizontal with the increase in surface temperature. The convergence over the summit of the hill is persistent during the period of surface heating. The laboratory study by Chen et al. (1996) and the two-dimensional numerical simulation of thermally induced mountain winds by Ye et al. (1987) also found such a vortex structure over the ridge. One can note that the convergence-induced vertical motion can disturb the adiabat at the 2-km level while the CBL depth is only about 1.2 km (Fig. 1b). The additional lifting of air induced by a hill may have the potential to trigger deep convection in the conditionally unstable atmosphere. Results from simulation A2 (not shown) indicate that the convergence over the hilltop and the vortex pair over both slopes are also evident and persistent. If the energy of the convergence-induced vertical motions could be converted entirely into potential energy, then the additional lifting of the inversion d caused by this terrain-induced convergence can be estimated by

$$d \sim w_t/N, \tag{5}$$

where w_t is taken as the intensity of the terrain-induced thermal circulation: this estimate is tested against the model and is presented in section 3c.

Figure 2a shows the maximum values of the vertical velocity over the hills, which are gathered from simulation A1 and A2 at different times. The maximum value of w over the hill during the time period examined is about 1.0 m s^{-1} in simulation A1 and about 3.5 m s^{-1} in simulation A2. Correspondingly, the maximum lifting of the air $d_{\max}$ is about 100 and 300 m in simulations A1 and A2, respectively. In the absence of moist processes, it is apparent that the additional lifting is relatively small. A minimum vertical velocity $w_{\min}$ for overcoming convective inhibition (CIN) can be approximately determined by $w_{\min} = \sqrt{2\text{CIN}}$. For the typical values of CIN of order 50 J kg^{-1}, the intensity of the dry thermal circulation may not be strong enough to lift air to the level of free convection. However, in practice the lifting is strongly sensitive to the latent heat release in shallow cumulus on one hand, and becomes significant as CIN $\rightarrow$ 0 on the other.

An estimate of the intensity of w_t can be derived based on the heat engine framework used by Souza et al. (2000). In the absence of cloud processes, w_t can be approximated by

$$w_t = \left(\frac{\eta c_p \Delta T_{\text{na}}}{\mu}\right)^{1/2}, \tag{6}$$

where c_p is the dry air specific heat, $\Delta T_{\text{na}} = (g/c_p)h + (T_{\text{d}} - T_{\text{b}})$ is the nonadiabatic temperature drop between the hilltop (hereafter point a) and the foot of the hill (hereafter point b), η is the thermodynamic efficiency of the convective circulation and μ is a dimensionless coefficient of dissipation of mechanical energy. The thermodynamic efficiency can be determined by (Souza et al. 2000)

$$\eta \approx g z_i / c_p \overline{T}, \tag{7}$$

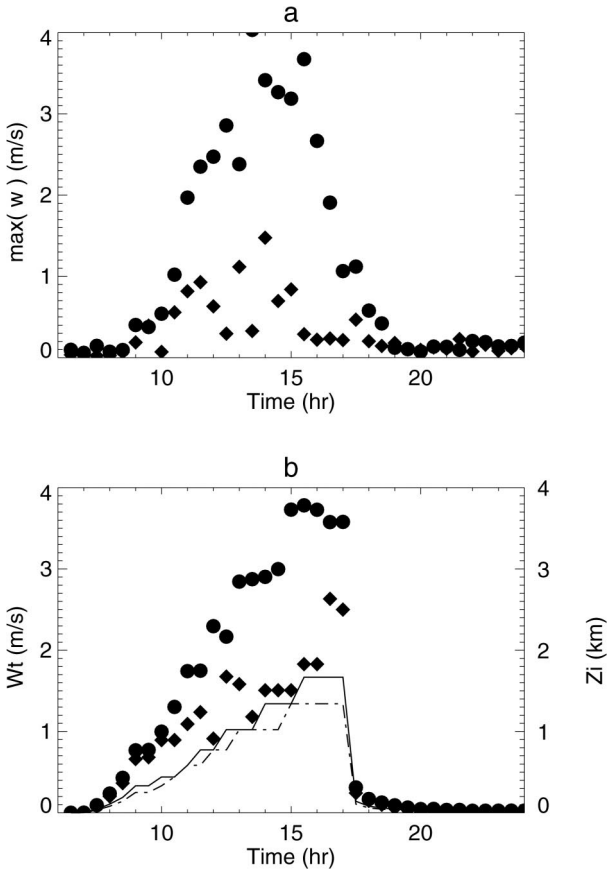

FIG. 2. The time evolution-of the maximum vertical velocity over the summit of hill in simulation A1 (filled ◊) and A2 (●): (a) the model results; (b) the formula predictions. The two lines in (b) represent the model-derived domain-averaged CBL depth in simulation A1 (dashed–dotted) and A2 (solid).

where z_i is the depth of the convective boundary layer, and $\overline{T}$ is the mean surface air temperature between points a and b. The coefficient of dissipation of mechanical energy is defined as (Renno et al. 1998)

$$\mu \equiv \frac{\oint f\, dl}{w^2}, \tag{8}$$

where f is the frictional force per unit mass and dl is an increment distance along the air parcels path. The dissipation of energy is mainly due to the turbulent viscosity $\nu \sim l_* w_*$, and μ can be parameterized as

$$\mu \sim \frac{\nu \nabla^2 w l_{\text{path}}}{w^2} \sim \frac{w_*^2 l_{\text{path}}}{w^2 l_*}, \tag{9}$$

where l_* and w_* are the eddy's characteristic length and velocity scales, and l_{path} is the integral path. Renno et al. (1998) has proposed that $w_* \sim 2w$ and $l_{\text{path}} \sim 4l_*$ by assuming that turbulence is homogeneous and isotropic, and that turbulent eddies are as energetic as the convective updraft, so that $\mu \sim 16$. For the convective eddies developed over a hill, it is here argued that where the topographic thermal circulation is dominant, it is appropriate to link the integral path l_{path} and the characteristic length scale l_* with both the CBL depth and the length of the hill slope. Inclusion of the hill slope as a controlling parameter is justified because in some circumstances we may expect coherent eddies to be linked directly to the topography. For relatively shallow hills, coherent eddies of relatively shallow aspect ratio may then be expected and are observed in numerical results. Note that, in some regimes, particularly at high mean wind, convective eddies remain relatively unaffected by topography (Tian and Parker 2002) and a form $l_{\text{path}} \sim 4l_*$ should be retained. For the topographic thermal regime, we assume $l_* \sim z_i$ and $l_{\text{path}} = 2(z_i + l_h)$, with l_h the slope length given by $l_h = h/\sin\beta$, β being the slope angle. Then, μ can be approximated by

$$\mu \sim 8\left(1 + \frac{l_h}{z_i}\right). \tag{10}$$

Substituting (7) and (10) into (6), we get a simple expression for the terrain-induced thermal circulation; that is,

$$w_t \approx \frac{1}{2}\sqrt{\frac{z_i}{2(z_i + l_h)}}(\eta_h g z_i + g' z_i)^{1/2}, \tag{11}$$

where $\eta_h = gh/c_p\overline{T}$, $g' = (\Delta T/\overline{T})g$, and $\Delta T = T_a - T_b$.

Figure 2b shows some values of w_t estimated from (11) based on the model results of simulations A1 and A2. Also shown are the depths of the CBL at different times in these two simulations (computed using a threshold stability). One can note from Fig. 2 that (11) gives a good estimation of the peak intensity of the thermally induced circulation over hills. Equation (11) also implies that w increases with the CBL depth z_i, and the higher a hill, the stronger the thermal circulation.

b. Baroclinic stagnation over hill

Under light wind conditions, the relative importance of the mechanical as opposed to the thermal forcing of a hill will determine the flow pattern over a hill. Figure 3 displays some model realizations from simulation B2. At the beginning of the simulation, when the surface thermal flux is relatively small, the flow pattern is mechanically dominated with downslope winds in the lee of the hill (Fig. 3a). A significant updraft associated with the leeward descent of the air is pushed downstream as the surface flux increases gradually (Fig. 3b). The underlying mechanism for this lee slope convergence could be explained by hydraulic theory: the supercritical flow over the lee slope passes into a subcritical flow downstream of the hill through a hydraulic jump (e.g., Turner 1973, 66–67).

At later afternoon from 1500 to 1800 UTC, the convective layer is well developed and significant upslope

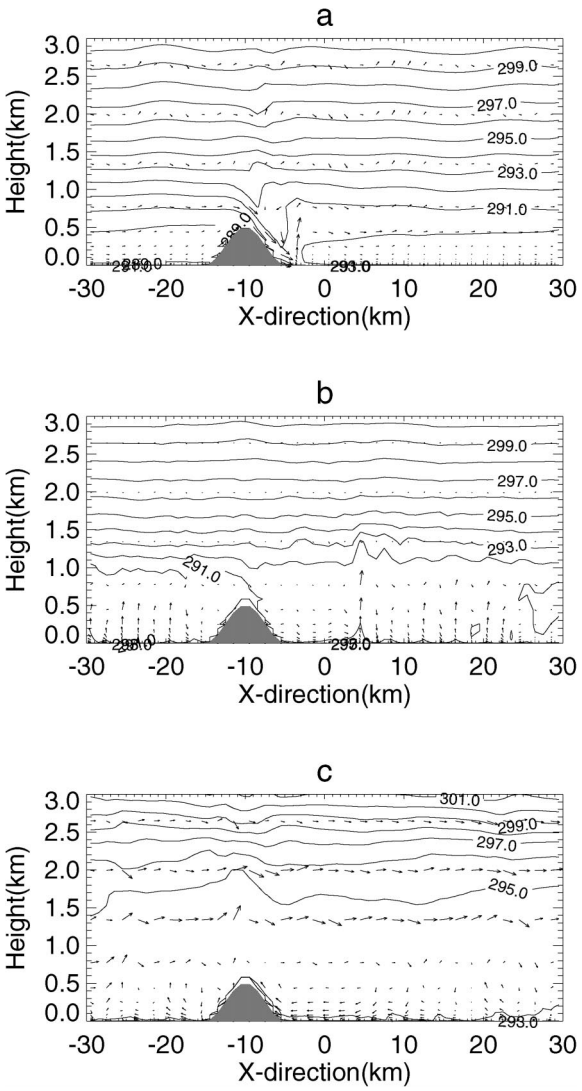

FIG. 3. The velocity and the potential temperature fields at (a) 0900, (b) 1100, and (c) 1730 UTC gathered from simulation B2. The contour interval for the potential temperature is 1.0 K.

winds can be observed in the lee of the hill. As an example, Fig. 3c shows the instantaneous potential temperature and wind vectors at 1730 UTC. The lifting of air by the terrain-induced thermal circulation is readily seen at the summit of the hill or slightly downwind of the peak. Note that the upslope winds over the windward slope are intermittent due to the presence of background winds.

The convective features in Fig. 3c, which are persistent over the hill in the later afternoon CBL, are typical of the convective core of observations over mountains (e.g., Raymond and Wilkening 1980). The physical mechanism of the convective core has been discussed by Tian and Parker (2002) based on the vorticity equation, and it is argued that the flow is controlled by a Richardson number Ri (based on a vorticity balance

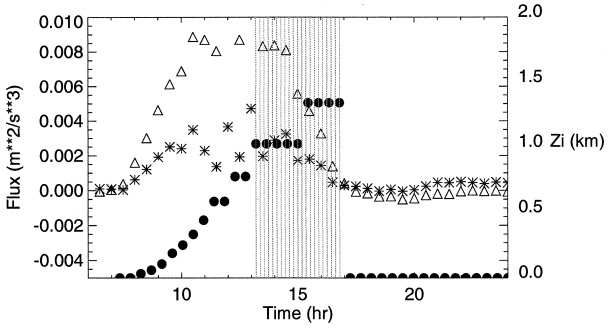

FIG. 4. The time evolution of the maximum surface sensible heat flux (triangles), CBL depth (dots), and flux anomaly (asterisks; defined as the difference between the maximum surface heat flux over the hill and the mean surface flux over the model domain).

between the inflow and the baroclinic source at the hill). Here we make further observations regarding the physical controls on the convective core, based on the diurnal cycle of its evolution in simulations B1 and B2, and relate these to external controlling parameters.

Figure 4 shows the time evolution of the surface sensible heat flux Q_s, CBL depth z_i, and flux difference $Q_d = Q_m - \overline{Q}_s$, where Q_m is the maximum surface heat flux over the hill, and $\overline{Q}_s$ is the mean surface flux over the model domain. The times at which a convective core appears in the model results are shaded on this plot. Evidence of the flow regimes in simulation B2 can be detected in Fig. 5, which shows the Hovmöller diagram of vertical velocities. It can be seen that, in the later afternoon, as thermal convection dominates, the convective eddies over the hill become stationary relative to the hill—this is the convective core. In the case of simulation B1, the convective eddies over the hill are less stationary and drift downstream of the hill without being blocked by the hill (not shown). Note that the convective core occurs in the later part of the day, after 1400 UTC, and persists for up to 1 h after the sensible heat flux has become negative. It should be realized that there is a maximum of sensible heat flux at the hill summit due to anomalously low evaporation (Tian and

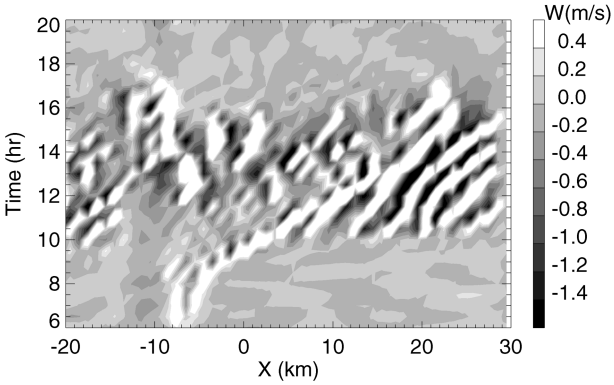

FIG. 5. The Hovmöller diagram of vertical velocity field from the simulation B2. The section is taken at 600 m AGL.

Parker 2002). When the flux difference over the hill is considered (Fig. 4) then the convective core is seen to break down at the time when the flux difference falls below zero.

The asymmetry of the convective core in time suggests that it occurs preferentially in a deeper boundary layer. In case study simulations of convective features (Tian et al. 2003), the model was found to initiate coherent convective structures around 1 h later than observed—this delay of convective onset in the model is not likely to explain the asymmetry in the daily cycle of the convective core.

Existence of the convective core requires the reversal of the near-surface flow in the lee of the hill; under strong basic-state winds this phenomenon is suppressed. The near-surface flow is also reduced for a given geostrophic wind in a deeper CBL relative to a shallower CBL, and this is an additional factor that will enhance the convective core in the afternoon. This flow reversal can occur through the baroclinic generation of strong upslope flow in the lee and through the existence of strong convective eddies, which may become coupled with the hill through its local heating maximum.

To quantify the above arguments we compare the upslope circulation in the lee with the influence of background flow on the maintenance of a steady circulation. Segal et al. (1987) showed that the circulation C_s associated with upslope winds can be estimated as

$$C_s = \frac{l}{\alpha} N^2 \frac{\partial Z_s}{\partial x} z_i, \tag{12}$$

where α is a Rayleigh friction coefficient [notation is here changed to be consistent with the present paper; Segal et al. (1987) also estimated z_i in terms of the integrated surface energy input]. Here we use this equation, following Tian and Parker (2002), to balance this circulation due to the upslope flow with the background circulation $C_0 = Ul$ over the same circuit. If the upslope circulation is stronger than that of the background state, then we can anticipate a reversed circulation in the lee, associated with the convective core over the hill. This condition of $C_s > C_0$ is then

$$F_c = \frac{N^2 \dfrac{\partial Z_s}{\partial x} z_i}{\alpha U} > 1. \tag{13}$$

This relation agrees with our numerical results in the following aspects.

1) In B2, the convective core appears at a critical z_i, apparently independent of the magnitude of surface fluxes (provided the flux anomaly is positive).
2) In B1, where $\partial Z_s/\partial x$ is a factor 0.4 smaller than in B2, with the other parameters of (13) unchanged, no convective core occurs.
3) In the A simulations, where U is a factor of 5 larger than in the B simulations, no convective core appears.

Note that the parameter α is a source of uncertainty for the quantitative use of F_c. In practice, the friction in the circulation will depend on roughness, stability, and other constraints.

The vertical velocities in the convective core (w_c) under considerably light wind conditions can still be roughly estimated by (11) with a small correction w_3, which is associated with wave motions over a hill; that is,

$$w_c = w_t + w_3. \tag{14}$$

The origins and intensity of w_3 are discussed in the next section.

c. Convection and wave interaction over a hill

The significant wave modification of convection over hills has been discussed by Tian and Parker (2002) based on model simulations over a periodic domain. Their results indicated that, under higher wind conditions, the terrain-induced gravity wave signature is visible until the CBL top is well above the hill top and the top of the CBL is modulated by those waves in the early stage of the CBL evolution. Before further analyzing the interaction between terrain-induced gravity waves and convection from simulations C1–C3, it is necessary to clarify when the terrain-induced waves are eroded away by convection and to what extent the CBL depth is modulated by the terrain-induced gravity waves. In an attempt to gain some perspective into these questions, the flow over hills is divided into two regions: a CBL region with $N = 0$, where a local equilibrium between convection and the main flow exists; and an upper region with stability N, where the perturbed flow is approximately adiabatic and can be described by the linear gravity wave equation. Thus, the interaction between gravity waves and convection can be discussed on the dynamic interface between these two regions, which, in the presence of thermal convection, could be taken as the top of the CBL, z_i.

Based on the two-layer framework here, waves and convection may interact with each other through matching the pressure perturbation and vertical velocity across the interface. Convective updrafts may also penetrate the interface to cause irreversible entrainment processes, and hence flatten the interface and weaken the waves above the CBL; these nonlinear processes are not addressed here.

To quantify the above considerations, Eqs. (2)–(4) are linearized into a wave equation in the limit of constant background wind speed U and stability

$$\frac{\partial^2 w}{\partial x^2} + \frac{\partial^2 w}{\partial z^2} + \left(\frac{N^2}{U^2}\right) w = 0. \tag{15}$$

Expressing vertical velocity w as a Fourier transform in horizontal wavenumbers, (15) becomes

$$\frac{\partial^2 \hat{w}}{\partial z^2} + \left(\frac{N^2}{U^2} - k^2\right)\hat{w} = 0. \quad (16)$$

Following standard analysis methods of linear gravity waves (e.g., Gill 1982), (16) has the solution of the form $\hat{w} = Ae^{-mz} + Be^{mz}$, where $m = \sqrt{k^2 - N^2/U^2}$ and A and B are constants determined by boundary conditions. In the CBL, where $N = 0$, thus $m = k$, the solution contains waves which are exponential in height and can be expressed in the form $\hat{w} = \hat{w}_1 e^{ikx-k(z+z_i)} + \hat{w}_2 e^{ikx+k(z+z_i)}$, where $\hat{w}_1$ and $\hat{w}_2$ are corresponding Fourier amplitudes of A and B, respectively. Note that, for mathematical convenience, the interface is at $z = 0$ and the surface is at $z = -z_i$. Above the CBL, when $k > N/U$, the solution is vertically evanescent, so the response is not of great interest here. When $k < N/U$, $\hat{w}$ has a plane wave solution with upward group velocity, so $\hat{w} = \hat{w}_3 e^{i[kx+\mu(z+z_i)]}$, where $\mu = \sqrt{N^2/U^2 - k^2}$ and $\hat{w}_3$ is the Fourier amplitude of vertical velocity on the interface. The terms $\hat{w}_1$, $\hat{w}_2$ and $\hat{w}_3$ can be determined by applying the linearized kinematic boundary condition at the surface and matching the vertical velocity and perturbation pressure at the interface. Now the Fourier amplitude of vertical velocity at the interface can be written as

$$\hat{w}_3 = \frac{\hat{Z}_s Uike^{kz_i}[1 - \tanh(kz_i)]}{e^{i\mu z_i}\left[1 - \dfrac{i\mu}{k}\tanh(kz_i)\right]}, \quad (17)$$

where $\hat{Z}_s$ is the Fourier amplitude of the orography. When linearized, the interface height $\hat{h}'$ is related to $\hat{w}_3$ through $\hat{h}' = \hat{w}_3/ikU$; then, the amplitude of $\hat{h}'$ can be written as

$$\hat{h}' = \frac{|\hat{Z}_s|e^{kz_i}[1 - \tanh(kz_i)]}{1 + (f_r^{-2} - 1)\tanh^2(kz_i)}, \quad (18)$$

where $\mathrm{Fr} = Uk/N$ is a Froude number. For practical use, Eq. (18) should be inverse Fourier transformed to retrieve the interface height in terms of the topographic height. Since we are concerned here with a simple scale analysis, we now consider the case of a periodic sequence of hills of the same shape as the isolated hill in the model. Notably, we are concerned with the flow in the vicinity of the hill itself, so we expect the amplitude of the flow properties not to be influenced greatly by the far field. This allows us to choose a characteristic wavelength for the hill. In the following discussion, $\hat{h}'$ is then an interface height scale.

Figure 6a demonstrates the variation of perturbation interface height in Fr and kz_i space. Note that the perturbation height decreases with kz_i quickly at low Froude numbers and decreases more slowly with kz_i at higher Froude numbers. Figure 6b is a plot of $\hat{h}'$ against z_i for $|\hat{Z}_s| = 500.0$ m and three different Froude numbers, that is, Fr = 0.10, 0.52, and 1.0. The term $\hat{h}'$ decreases rapidly with z_i; however, the variation of $\hat{h}'$ with Fr is not linear as it is also controlled by k. Consistent with the model results of simulation C2, in which Fr has a value of about 0.52 ($k = 2\pi/l$), Fig. 6b indicates that the perturbation of the CBL depth z_i by the terrain-induced waves is still significant when z_i reaches 2 km, which is much greater than the maximum height of the orography under consideration. Under light wind conditions, as in simulation B2, Fr is small (~0.1), so w_3 only has a small contribution in (14) and perturbation of the CBL top is dominated by thermal circulation induced by orography. These linear predictions quantitatively agree with our model results, and more discussions can be found in the next section with respect to simulations C1, C2, and C3.

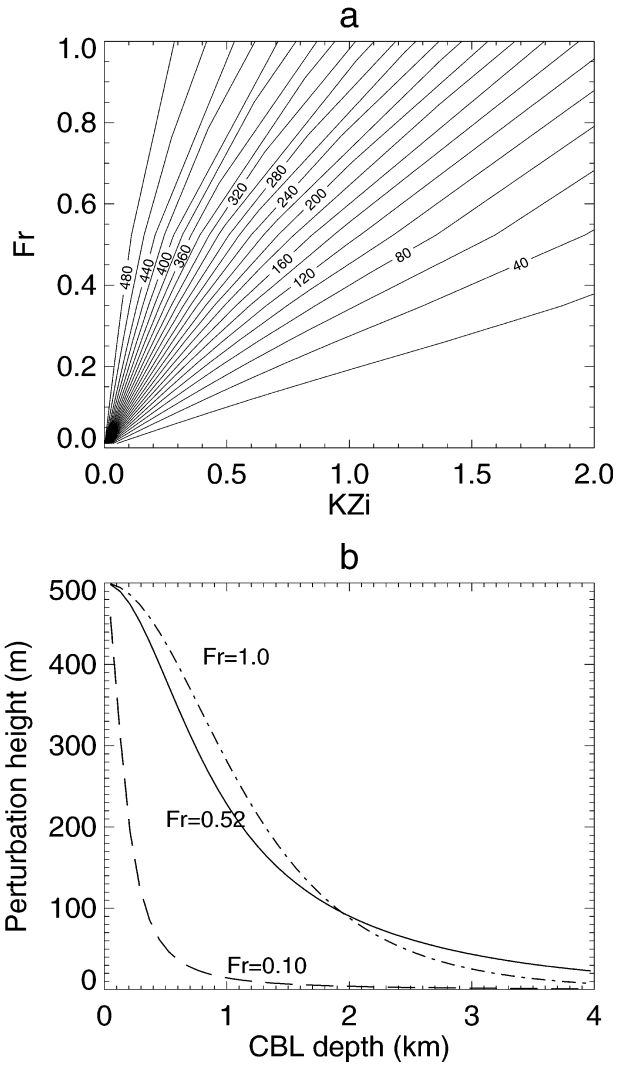

FIG. 6. The variation of the perturbation height (a) in Fr and lz_i space and (b) to the CBL depth z_i for a hill with a maximum height of 500 m. Three lines correspond to different Froude numbers.

At this stage, it is necessary to compare the model-derived perturbations z_i' to the CBL depth z_i with the corresponding formula-estimated values. By assuming that the CBL top is where the gradient of the potential

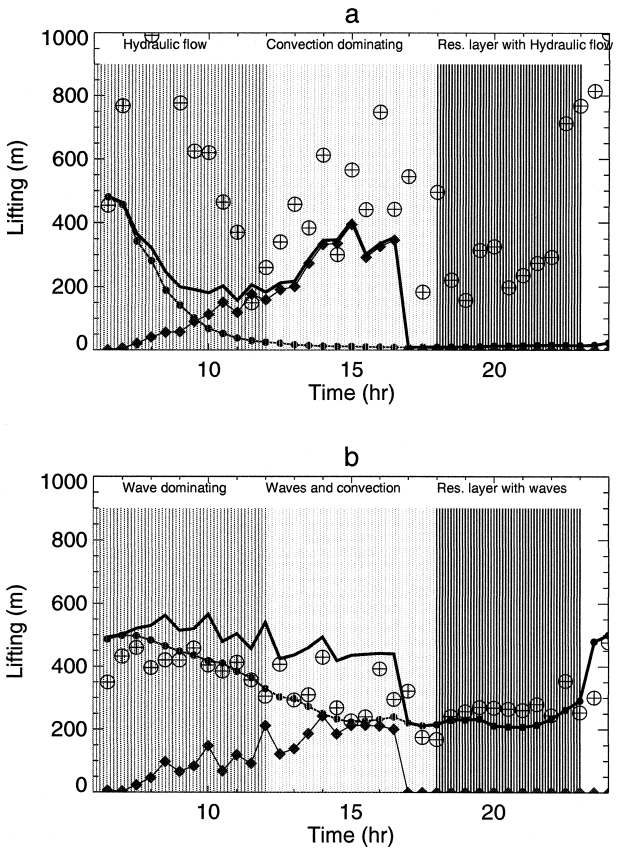

FIG. 7. The time variation of perturbation heights z_i' estimated by different method using the model results from (a) simulation B2 and (b) simulation C2. The thermal lifting height (w_t/N) is represented by diamond lines, linear wave perturbations ($\hat{h}'$) is represented by dotted lines, and the heavy solid line is for $\hat{h}' + w_t/N$. The symbol $\oplus$ stands for values of z_i' calculated from the model potential temperature field. Characteristic flow patterns at different times are marked at the tops of (a) and (b).

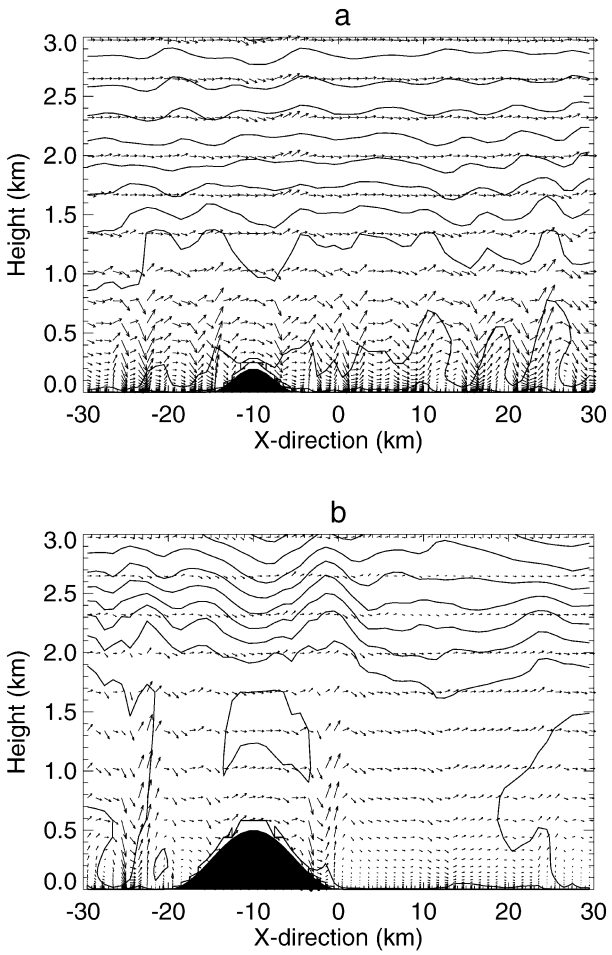

FIG. 8. The realizations of the wind field (vectors) and the potential temperature field (solid lines) at 1400 UTC from simulation (a) C1 and (b) C3. The contour interval is 1 K for the potential temperature.

temperature is less than a critical value, we can first estimate z_i and z_i' from the model potential temperature field. Using these z_i values, wave perturbations can be calculated from (14) while the thermal lifting height can be approximated using (5). Then, one can expect that the total perturbation $w_t/N + \hat{h}'$ may approximate the model-derived value z_i'. Figure 7 shows some results obtained from simulation B2 and C2. It is apparent that when the flow is wave dominated, the linear wave theory gives a good estimation of the perturbation height z_i' (Fig. 7b), within approximately 50 m, or around 5% of z_i. When the flow is convectively dominated (Fig. 7a), w_t/N appears to underestimate the peak perturbations to the interface height over the hill, despite the close agreement between model and predicted w_t seen in Fig. 2. This underestimation may be due to difficulties in objectively defining z_i in the convective regime, or perhaps due to the oversimplification of the energetic arguments leading to (5). If waves and convection coexist, $w_t/N + \hat{h}'$ is impressively consistent with the model-derived values of z_i' (Fig. 7b). In situations where hydraulic flow dominates, both linear wave theory and heat engine approach give a poor prediction of z_i' as expected.

4. Downstream modification of convection

It is known that convection itself could also trigger internal gravity waves. Some previous work has investigated the interaction between those thermally induced waves and the CBL (e.g., Carruthers and Moeng 1987; Clark et al. 1986; Weinstock 1987), and their results suggested that resonance can be expected where convective eddies have the same wavelength as the overlying waves just above the CBL.

Figure 8 displays the instantaneous velocity field and potential temperature field at 1400 UTC gathered from simulation C1 and C3. It is evident that a 200-m-high hill with a width of 10 km has small effects on the convection: the wavelength and the amplitude of the convective eddies in Fig. 8a are not significantly different from corresponding results in the flat domain simulation (not shown), and only those eddies just over the

hill are slightly disturbed. In the case of simulation C3 (Fig. 8b), there are only two strong convective eddies in the model domain, and the convective layer reaches about 2 km, which is approximately 500 m deeper than that in Fig. 8a. The corresponding results from simulation C2 (not shown) indicate that the CBL is about 1.5 km deep, and there are more eddies in the domain compared with those in Fig. 8b. The results here suggest that the terrain-induced gravity waves with wavelength larger than that of convective eddies tend to suppress some of the eddies to force the thermal eddy wavelength more in accordance with the hill length and tend to make the convective updrafts stronger. If the hill length is closer to the convective eddy wavelength, as in simulations C1 and C2, although resonance between waves and convective eddies is likely to occur, the CBL depth is not significantly changed by lee waves.

More evidence on the modification of the CBL energy distribution by the gravity waves can be gained from Fig. 9, which shows the mean potential temperature profiles (averaged from half-hourly realizations from 1100 to 1600 UTC) at 10 and 40 km from the upstream boundary for simulations C1, C2, and C3. One can note the potential temperature profiles are quite different between simulations C1, C2, and C3 both down- and upstream of the hills. The CBL potential temperature for simulation C1 is the smallest. Possible reasons for these differences are that the eddy structures in each case are different (as in Gopalakrishnan et al 2000), leading to differing entrainment rates, or that the total CBL volumes (subtracting the differing hill volumes in each case) are different between cases, so that the heat input is mixed through a larger CBL volume in case C1. In case of simulation C3, the profiles up- and downstream of the hill are also different: air upstream of the hill is well mixed and the time-averaged mixed layer is much deeper than that downstream of the hill. It should be pointed out that the domain-averaged potential temperature profiles have little difference between different simulations.

The surface equivalent potential temperature θ_e obtained from simulation C2 (not shown) indicates that the surface θ_e is significantly higher at the foot of the hill from 1000 to 1500 UTC, associated with the persistent descent of air from the hilltop. Consistent with that of potential temperature, θ_e upstream and further downstream of the hill is not significantly different in this case.

While significant orographic modification of convection by gravity waves can be readily seen from simulations C2 and C3, another kind of downstream modification can be detected from simulation B2. One can note from Fig. 5 that the vertical motions are first triggered in the lee of the high hill in the early morning, while there are no significant thermal eddies elsewhere until 1000 UTC. These orogenic eddies are advected downwind by the mean flow before the thermal convection is developed over the whole model domain. The

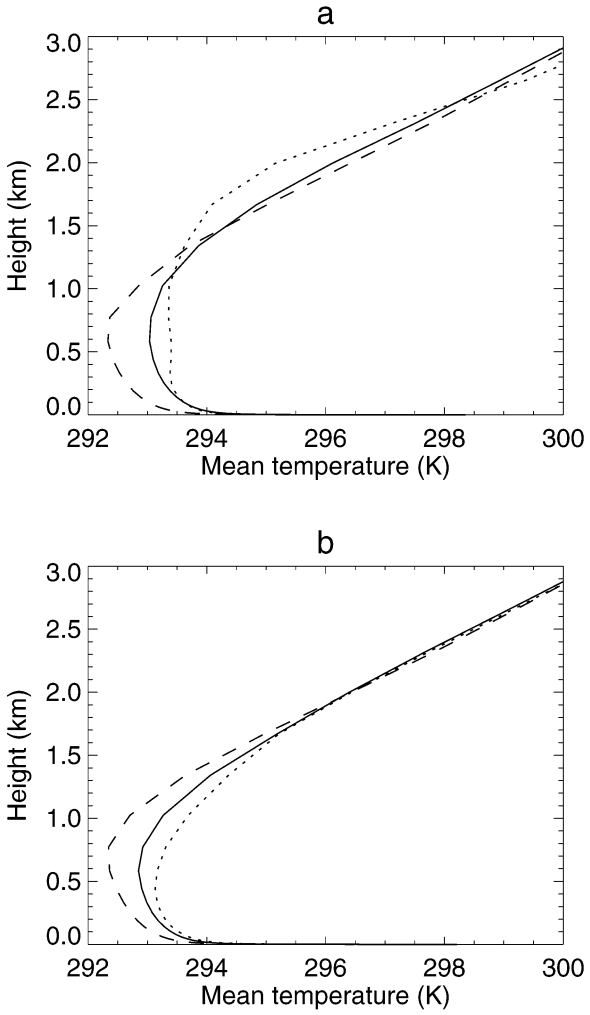

FIG. 9. The time-averaged (from 1100 to 1600 UTC) potential temperature (a) upstream 10 km and (b) downstream 20 km of the hills in simulation C1 (dashed lines), C2 (solid lines), and C3 (dotted lines).

thermal convective eddies appear to be intensified when orogenic eddies in the lee of the hill propagate downstream and finally meet the thermal convective cells. Also, the convective eddies at a distance greater than 10 km from the foot of the hill are well developed and seem to be less affected by the hill, while those eddies within a distance of 10 km from the hill are relatively weak and may suggest orographic modification of those eddies. It appears that, although the persistent thermal circulation over the lee slope could induce convergence at the summit of a hill, convective eddies just downstream of the hill ($X < 10$ km) are likely to be suppressed by the reversed flow and compensating downdraft downstream of the hill.

5. Conclusions and discussion

Shallow boundary layer convection over a single hill has been studied in the context of the diurnal thermal

cycle with much attention paid to daytime convection. Although the unsteadily forced model solution may be sensitive to the initial conditions, for short-period simulations, which are performed in appropriate model parameter space, general insights into the issue can still be obtained.

Under a motionless background state, the flow response to a heated obstacle is a vortex pair with one over each slope. The corresponding convergence over the summit of a hill will result in an additional lifting of the inversion, which is proportional to w_t/N in continuously stratified flow, and w_t increases with the CBL depth and hill height. In the absence of moist processes, the additional lifting is not large relative to typical CIN values; however, if shallow cumulus heating was included in the model, this lifting would be increased and has potential importance in triggering deep convection. The lifting depends principally on the background profiles of wind and stability, the hill height and the surface thermal forcing.

Some results concerning the occurrence of the convective core have also been presented. This phenomenon is found to occur in the late afternoon, when the CBL top is high, and occurs preferentially over high hills under light background winds. Simple quantification of this behavior in terms of *external* parameters has led to the derivation of a nondimensional parameter F_c, which relates the upslope circulation in the lee to the background wind shear. This parameter is found to explain the existence of the convective core in our set of numerical results. Since the convective core may be an important feature in terms of triggering of moist convection, further work to test this parameter is recommended.

When the terrain-induced waves are significant, the modification of convection by these waves is pronounced over hills. The linear gravity wave analysis based on a two-layer atmosphere reveals that the wave modification of convection is determined by a Froude number Fr ($=Uk/N$) and the interface height between the CBL and the overlying stable layer, that is, the CBL height z_i. The magnitudes of perturbations to the interface by waves increase with the height of a hill, but decrease rapidly with z_i and vary significantly with Fr. If waves and convection coexist, $w_t/N + \hat{h}'$ is consistent with the model-derived perturbation heights to the CBL top z_i.

In testing the simple estimates against the numerical model, the limitations of the modeling approach need to be reiterated. This model has only coarse resolution of convective eddies, due to the mesoscale domain size, and therefore has imperfect representation of turbulent transports and also of entrainment processes at the CBL top. The effect of entrainment may, in reality, be to suppress variations in CBL depth forced, for example, by gravity wave motions, but LES modeling is probably required to address this issue. What the model can show is that the very simple scale analysis shows some useful skill even against a complex nonlinear numerical solution of the equations.

The diagnosis of downstream modification of convection by a single hill is not easy to quantify using model results due to the contamination of model solutions by open lateral boundary conditions. However, with careful selection of the model domain and boundary schemes, general physical properties of a model solution could be retained in the interior of a model domain. The modification of the CBL by an isolated hill exists in two aspects: the terrain-induced waves modulate the CBL top through coupling between these waves and the underlying convective eddies; these waves can also modify the energy distribution in the CBL and hence change the eddy number and strength, and hence the CBL depth. Downstream modification can even be observed in the absence of significant lee waves, related to the prevailing upslope flow in the lee of hill and the compensating downward flow. The surface equivalent potential temperature is relatively high at the lee foot of the hill but low over the summit. Particularly noticeable is that hills have a significant impact on the vertical profiles of potential temperature up- and downstream of hills.

Acknowledgments. Wenshou Tian has been supported by an Overseas Research Scholarship. We would like to thank three anonymous reviewers for useful and thorough comments.

REFERENCES

Akaeda, K., J. Reisner, and D. Parsons, 1995: The role of mesoscale and topographically induced circulations in initiating a flash flood observed during the TAMEX project. *Mon. Wea. Rev.,* **123,** 1720–1739.

Carruthers, D. J., and C.-H. Moeng, 1987: Waves in the overlying inversion of the convective boundary layer. *J. Atmos. Sci.,* **44,** 1801–1808.

Chen, R.-R., N. S. Berman, D. L. Boyer, and H. J. S. Fernando, 1996: Physical model of diurnal heating in the vicinity of a two-dimensional ridge. *J. Atmos. Sci.,* **53,** 62–85.

Chu, C.-M., and Y.-L. Lin, 2000: Effects of orography on the generation and propagation of mesoscale convective systems in a two-dimensional conditionally unstable flow. *J. Atmos. Sci.,* **57,** 3817–3837.

Clark, T. L., T. Hauf, and J. P. Kuettner, 1986: Convectively forced internal gravity waves: Results from two-dimensional numerical experiments. *Quart. J. Roy. Meteor. Soc.,* **112,** 899–925.

Crook, N. A., T. L. Clark, and M. W. Moncrieff, 1990: The Denver Cyclone. Part I: Generation in low Froude number flow. *J. Atmos. Sci.,* **47,** 2725–2742.

Davies, H. C., 1983: Limitations of some common lateral boundary schemes used in regional NWP models. *Mon. Wea. Rev.,* **111,** 1002–1012.

Gill, A. E., 1982: *Atmosphere–Ocean Dynamics.* Academic Press, 662 pp.

Gopalakrishnan, S. G., S. B. Roy, and R. Avissar, 2000: An evaluation of the scale at which topographical features affect the convective boundary layer using large eddy simulations. *J. Atmos. Sci.,* **57,** 334–351.

Lin, Y.-L., and T.-A. Wang, 1996: Flow regimes and transient dy-

namics of two-dimensional stratified flow over an isolated mountain ridge. *J. Atmos. Sci.*, **53,** 139–158.
McNider, R. T., and R. A. Pielke, 1981: Diurnal boundary-layer development over sloping terrain. *J. Atmos. Sci.,* **38,** 2198–2212.
Raymond, D. J., and M. Wilkening, 1980: Mountain-induced convection under fair weather conditions. *J. Atmos. Sci.,* **37,** 2693–2706.
Renno, N. O., M. L. Burkett, and M. P. Larkin, 1998: A simple thermodynamical theory for dust devils. *J. Atmos. Sci.,* **55,** 3244–3252.
Rowell, D. P., and J. R. Milford, 1993: On the generation of African squall lines. *J. Climate,* **6,** 1181–1193.
Segal, M., Y. Ookouchi, and R. A. Pielke, 1987: On the effect of steep slope orientation on the intensity of daytime upslope flow. *J. Atmos. Sci.,* **44,** 3587–3592.
Smith, R. B., and Y.-L. Lin, 1982: The addition of heat to a stratified airstream with application to the dynamics of orographic rain. *Quart. J. Roy. Meteor. Soc.,* **108,** 353–378.
Smolarkiewicz, P. K., R. M. Rasmussen, and T. L. Clark, 1988: On the dynamics of Hawaiian cloud bands: Island forcing. *J. Atmos. Sci.,* **45,** 1872–1905.
Souza, E. P., N. O. Renno, and M. A. F. Silva Dias, 2000: Convective circulations induced by surface heterogeneities. *J. Atmos. Sci.,* **57,** 2915–2922.
Tian, W.-S., and D. J. Parker, 2002: Two-dimensional simulation of orographic effects on mesoscale boundary layer convection. *Quart. J. Roy. Meteor. Soc.,* **128,** 1929–1952.
——, ——, and C. A. D. Kilburn, 2003: Observations and numerical simulation of atmospheric cellular convection over mesoscale topography. *Mon. Wea. Rev.,* **131,** 222–235.
Tripoli, G. J., and W. R. Cotton, 1989: Numerical study of an observed orogenic mesoscale convective system. Part I: Simulated genesis and comparison with observations. *Mon. Wea. Rev.,* **117,** 273–304.
Tucker, D. F., and N. A. Crook, 1999: The generation of a mesoscale convective system from mountain convection. *Mon. Wea. Rev.,* **127,** 1259–1273.
Turner, J. S., 1973: *Buoyancy Effects in Fluids.* Cambridge University Press, 368 pp.
Walko, R. L., W. R. Cotton, and R. A. Pielke, 1992: Large-eddy simulations of the effects of hilly terrain on the convective boundary layer. *Bound.-Layer Meteor.,* **58,** 133–150.
Weinstock, J., 1987: The turbulence field generated by a linear gravity wave. *J. Atmos. Sci.,* **44,** 410–420.
Ye, Z. J., M. Segal, and R. A. Pielke, 1987: Effects of atmospheric thermal stability and slop steepness on the development of daytime thermally induced upslope flow. *J. Atmos. Sci.,* **44,** 3341–3354.